

MODELLING AN ELECTRO-HYDRAULIC POPPET VALVE

Patrick Opdenbosch¹, Nader Sadegh², Wayne Book², Todd Murray³ and Roger Yang³

¹Machine Technologies Research, Technology and Solutions Division, Caterpillar Inc., Peoria, IL 61656, USA

²The George W. Woodruff School of Mechanical Engineering, Georgia Institute of Technology, 813 Ferst Dr., Atlanta, GA 30332, USA

³HUSCO International, 2239 Pewaukee Rd, Waukesha, WI 53188, USA

opdenbosch_patrick@cat.com, nader.sadegh@me.gatech.edu, wayne.book@me.gatech.edu, todd.murray@huscointl.com,
roger.yang@huscointl.com

Abstract

This paper develops the dynamic modelling of a novel two-stage bidirectional poppet valve and proposes a simplified model that is more suitable for control purposes. The dynamic nonlinear mathematical model of this Electro-Hydraulic Poppet Valve (EHPV) is based on the analysis of the interactions among its three internal systems: the mechanical, hydraulic, and electromagnetic system. A discussion on the employed experimental methodology is included along with the validation of this model. When the pressure differential across the valve is sufficiently high and does not vary considerably, the model for this valve can be simplified substantially. More specifically, the EHPV can be modelled as a linear second order system with a static input nonlinearity. This nonlinearity is realized from the valve's steady state characteristics. The advantage of this separation between valve dynamics and nonlinearities is that an inverse linearisation approach (to cancel the nonlinearity) can be used to facilitate the control task for the valve.

Keywords: nonlinear model, proportional control valve, poppet valves, bidirectional valve, flow conductance factor

1 Introduction

Proportional control valves are widely employed for motion control in fluid power applications. Research and developments that include the characterization of flow area and flow forces on poppet valves (Johnston et al., 1991), stability analyses (e.g. Shin, 1991; Hayashi, 1995), implementation of electro-hydraulic controls (e.g. Kitagawa et al., 1998; Du, 2002) among others are now permitting poppet-type cartridge valves to be considered in this category of control units. One of these new alternatives is the Electro-Hydraulic Poppet Valve (EHPV) considered in this paper. This valve has been designed and manufactured by HUSCO International to implement the independent metering concept for motion control of hydraulic actuators (Tabor, 2004).

Aside from the corresponding patents, little can be found about this valve in the open literature. The purpose of this paper is then to develop and simulate a nonlinear mathematical model for the EHPV¹. In addition,

a simplified model will be presented, which is more suitable for controller development.

The EHPV, shown in Fig. 1 and described in (Yang et al., 2001; Yang et al., 2004; Opdenbosch et al., 2004), is a valve that opens proportionally to the amount of current sent to its solenoid. Among its distinguishing features, this valve possesses an internal pressure compensation mechanism. This mechanism ensures that the amount of current needed to initially open the valve is always consistent. Moreover, this valve has virtually zero leakage (less than 0.5 cc/min), it is bidirectional, and has low hysteresis (less than 5%) (Yang et al., 2001; Yang et al., 2004). In addition to the previously outlined assets, poppet valves in general offer high resistance to contaminants, high flow area to poppet displacement ratios, excellent sealing capabilities, low cost, and low maintenance. Moreover, when compared to other control valves (such as spool valves), poppet valves require less strict machining tolerances (Roberts, 1988; Johnston et al., 1991).

Poppet valves are difficult to model because of their nonlinear characteristics. Flow coefficients, fluid flow, and flow forces in single-stage conical poppet valves

¹ The valve considered in this paper is designed for 151 L/min (40 GPM) at 1.5 MPa with an opening bandwidth of 5 Hz.

were initially investigated in (Johnston et al., 1991, Vaughan et al., 1992). The flow characteristics of a pulse-width-modulated (PWM) controlled single-stage poppet valve were studied by (Kitagawa et al., 1998). More recently, a model-based approach was used to investigate the limitations of the “Valvistor”, a valve similar to the one considered herein (Zhang et al., 2002). Further research in terms of the stability and performance of this valve was presented in (Fales, 2006). In addition, EASY5 was employed to characterize the dynamic behavior of the Valvistor in (Liu et al., 2002). Additionally, it was concluded in (Liu et al., 2002) that the response of the Valvistor can be approximated by a linear dynamic system followed by a static nonlinearity. It will be shown in this paper that a similar idea applies for the EHPV. More specifically, the EHPV can be modeled as a linear second order system with a static input nonlinearity. This nonlinearity is realized from steady state data collected experimentally. The advantage of this separation between valve dynamics and nonlinearities is that an inverse linearisation approach can be used to cancel the nonlinear part and facilitate the control task for the valve.

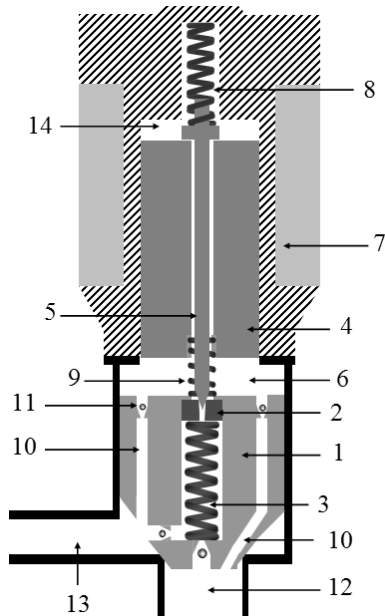


Fig. 1: Diagram of the Electro-Hydraulic Poppet Valve

The rest of the paper is organized as follows. The working principle of the EHPV is presented first followed by the development of the dynamic model of the valve. Next, the experimental technique used in the validation of the nonlinear model is discussed. This is followed by the validation results. A simplified mathematical model of the EHPV is presented afterwards. The concluding remarks are given at the end accompanied by the acknowledgements and references.

2 Working Principle

In simple terms, the EHPV is used to control fluid flowrate or fluid pressure. This is achieved by changing the restriction the valve imposes on the flow. However,

from a numerical point of view, it is easier to manipulate the valve in terms of its flow conductance factor², K_v . As a result, this valve is viewed herein as a system whose input is the current sent to the solenoid and whose output is its flow conductance coefficient K_v . The relationship among the flowrate through the valve Q , the pressure difference across the valve ΔP , and the valve's flow conductance is given in Eq. 1.

$$Q|Q| = K_v^2 \Delta P \quad (1)$$

The procedure in which the EHPV opens is explained next following the numbering scheme appearing in Fig. 1. The first stage of the valve houses the main poppet element 1 and the pressure compensation mechanism. This mechanism consists of a piston 2 and a tubular spring 3. The second stage houses an armature 4 and a pilot pin 5. A control pressure chamber 6 separates these two stages. Other components of the EHPV include the pilot head chamber 14, the modulating spring 8, the bias spring 9, check valves 11, the ‘nose’ connection port 12, and the ‘side’ connection port 13. In order to achieve flow through the valve, high-pressure flow (inflow) is conducted through a small passage 10 in the main poppet to the control chamber. When the solenoid 7 is activated, the pilot pin is pulled and pilot flow is allowed to go from the control pressure chamber through the piston and tubular spring to the low pressure side. This action lowers the pressure in the control pressure chamber. By lowering the pressure in this chamber, a force imbalance is created on the main poppet. This effect enables the displacement of the main poppet away from the valve seat. Consequently, a direct passage between the inlet and outlet connections of the valve is established. The valve's bidirectional capability resides in the fact that the control pressure chamber receives high-pressure flow from either port of the valve (Yang et al., 2001).

The compensation mechanism is briefly described next. As the pressure differential across the main poppet increases, the piston and tubular spring are compressed. This results in the relaxation of the modulating spring preload force acting on the pilot pin. This action compensates the increasing hydraulic load on the pilot pin (Yang et al., 2001, Yang et al., 2004).

3 Nonlinear Mathematical Model

The model of the EHPV is constructed by taking into account the interactions among its three internal systems: the mechanical, hydraulic, and electromagnetic systems. The internal electromagnetic system is discussed first. This system receives the input of the EHPV whether it is the voltage applied to the solenoid or the current going through the same. If the former is the case, then the solenoid can be modeled as an RL-circuit with varying inductance (See for example Vaughan and Gamble, 1996, Kajima and Kawamura,

² When the valve is closed, the conductance is zero while the restriction is ∞ . The flow conductance parameter is a positive quantity and it is the reciprocal of flow restriction.

1995). In this paper, the second case applies. This means that there is a servo controller that is used to control the current passing through the solenoid. As such, the nonlinear electromagnetic effects, other than the solenoid's force characteristics which are determined experimentally, are ignored in this system. This force, which is a function of the gap and the solenoid current, is found experimentally and implemented into the model with the aid of a look-up table. The gap x is defined to be

$$x = y_{p,\max} - y_p \quad (2)$$

where y_p represents the position of the armature-pilot and $y_{p,\max}$ denotes the maximum displacement of the same.

The mathematical model of the internal mechanical system, shown in Fig. 2, is considered next. It is not difficult to see that a force balance on the main poppet yields

$$\begin{aligned} m_{mp} \ddot{y}_{mp} = & -b_b (\dot{y}_{mp} - \dot{y}_p) - b_c (\dot{y}_{mp} - \dot{y}_c) - F_{b,pl} \\ & - k_b (y_{mp} - y_p) + F_{Hmp} + F_{Rmp} - \mu_{mp} \\ & - b_{mp} \dot{y}_{mp} - [k_c (y_{mp} - y_c)] (y_{mp} - y_c) \end{aligned} \quad (3)$$

where m_{mp} is the mass of the main poppet, $F_{b,pl}$ represents the bias spring preload and F_{Rmp} accounts for all reaction forces due to displacement constraints. The variable μ_{mp} is included to account for friction forces due to the presence of dynamic seals. Note that $k_c(\cdot)$, the stiffness of the tubular spring, is written as a function of the relative displacement $y_{mp} - y_c$ to account for nonlinearities. The variable F_{Hmp} represents the net hydraulic force acting on the main poppet due to the interactions with the fluid in contact. As such,

$$\begin{aligned} F_{Hmp} = & P_A A_A + P_B A_B - P_p A_{mpup} \\ & - P_c A_{mplow} - f_{flow,mp} \end{aligned} \quad (4)$$

where A_A is the effective area of the main poppet wetted by the pressure at port A, P_A . Moreover, A_B is the effective area wetted by the pressure at port³ B, P_B . In this equation, $f_{flow,mp}$ accounts for flow forces exerted upon the main poppet. In addition, A_{mpup} is the effective area of the main poppet wetted by the control chamber pressure, P_p . Finally, A_{mplow} is the effective area of the main poppet wetted by the pressure P_c in the tubular spring cavity. Note that the pressures appearing in the above equation are all static pressures.

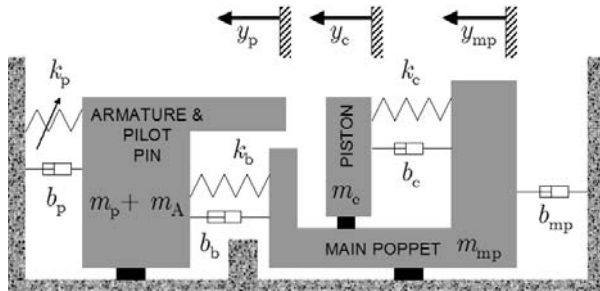


Fig. 2: Model of the internal mechanical system

³ In this paper, the 'side' connection is labeled port A while the 'nose' connection is labeled port B.

A force balance on the compensating piston is given by

$$\begin{aligned} m_c \ddot{y}_c = & b_c (\dot{y}_{mp} - \dot{y}_c) + [k_c (y_{mp} - y_c)] (y_{mp} - y_c) \\ & + F_{Rc} + F_{Hc} - \mu_c \end{aligned} \quad (5)$$

where m_c is the mass of the tubular spring and piston, F_{Rc} accounts for all reaction forces due to displacement constraints. The variable μ_c is included to account for friction forces, caused by the presence of dynamic seals. The variable F_{Hc} represents the net hydraulic force acting on the compensating piston. As such,

$$F_{Hc} = P_c A_{c,low} - P_p A_{c,up} - f_{flow,c} \quad (6)$$

where the variables $A_{c,up}$ and $A_{c,low}$ represent the effective areas of the piston that are wetted by the corresponding pressures. The variable $f_{flow,c}$ accounts for flow forces exerted upon the compensating piston.

Finally under the assumption that the armature and the pilot pin remain in contact at all times,

$$\begin{aligned} (m_A + m_p) \ddot{y}_p = & -b_p \dot{y}_p - k_p y_p - F_{m,pl} + F_{b,pl} \\ & + b_b (\dot{y}_{mp} - \dot{y}_p) + k_b (y_{mp} - y_p) \\ & + F_{Rp} + F_{Hp} - \mu_p + F_{sol} \end{aligned} \quad (7)$$

where m_A is the mass of the armature, m_p is the mass of the pilot pin, F_{sol} is the electromagnetic force that the solenoid exerts on the armature, $F_{m,pl}$ is the modulating spring preload (manually adjustable), and F_{Rp} accounts for all reaction forces due to state constraints. The variable μ_p is included to account for friction forces (due to dynamic seals). The variable F_{Hp} represents the net hydraulic force acting on the pilot pin and armature. As such,

$$F_{Hp} = P_p A_{p,low} - f_{flow,p} - P_h A_{p,up} + P_c A_o \quad (8)$$

where the variables $A_{p,up}$ and $A_{p,low}$ represent the effective areas of the armature-pin body that are wetted by the corresponding pressures. In particular, A_o is the cross-sectional area of the pilot pin that makes contact with the aperture in the compensating piston when the valve is closed. The variable $f_{flow,p}$ accounts for flow forces exerted upon the armature-pin body.

It is important to mention that the reaction forces mentioned previously, resulting from displacement constraints, are implemented using *positive* spring-dampers. These spring-dampers exert a repelling and dissipative force and are turned on only when the corresponding bodies collide.

The mathematical model of the internal hydraulic system is considered next. This hydraulic model is given in Fig. 3. This system is represented by fixed and variable orifice type models with internal pressure chambers. In this figure, the pressure chambers are labeled "P", "C", and "H", corresponding to the control pressure chamber, the compensation chamber, and the pilot head chamber respectively. As its name suggests, the pressure in chamber "P" is the means to control the opening of the main poppet. In addition, chamber "H" fills with oil to reduce the hydraulic imbalance on the pilot-armature body. Chamber "C" represents the volume of oil inside the tubular spring. In addition, this diagram shows the connection ports labeled as A and B

and the corresponding flow coefficients for each flow path (e.g. K_{VCA} is the flow conductance coefficient for the flow going from chamber C to port A, denoted by Q_{CA}).

By convention, the flow from A to B is called *forward* flow. On the other hand, the flow from B to A is called *reverse* flow. These are considered as the main flows of the valve. In either case, the total flow through the valve is composed by pilot and main flow. In the forward flow case for instance, pilot flow is conducted through the left-most check valve in Fig. 3 and the K_{VAP} orifice to the "P" chamber, from which it is conducted to the "H" chamber. As the armature-pilot is displaced, hydraulic fluid flows from the "P" chamber to the "C" chamber. A check valve prevents the fluid from going to the high-pressure side (port A) and the fluid goes to the low-pressure port (port B) through the K_{VCB} orifice.

The flow network inside the EHPV is modeled with the assumption that fluid inertance is negligible due to the geometry of the flow passages. In addition, changes in pressure due to height differences are also neglected. It can be observed from Fig. 3 that three types of flow models are considered: *two-way* corresponding to Q_{PH} , *one-way* corresponding to Q_{AP} , Q_{BP} , Q_{CA} , Q_{CB} , and *variable* corresponding to Q_{PC} and Q_{AB} . With these assumptions, the two-way flow is computed from Eq. 9.

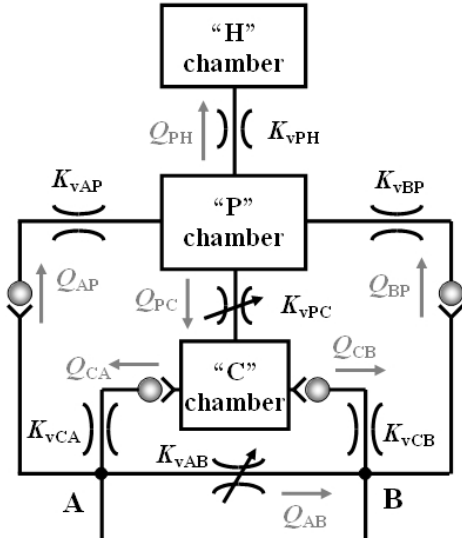


Fig. 3: Model of the internal hydraulic system

$$Q_{PH} = K_{VPH} \operatorname{sgn}(P_p - P_h) \sqrt{|P_p - P_h|} \quad (9)$$

$$\operatorname{sgn}(\bullet) = \begin{cases} +1 & \bullet > 0 \\ -1 & \bullet < 0 \\ 0 & \bullet = 0 \end{cases}$$

In addition, the one-way flow models are given by

$$Q_{ij} = K_{vij} \Lambda(P_i - P_j) \sqrt{|P_i - P_j|} \quad (10)$$

$$\Lambda(\bullet) = \begin{cases} 1 & \bullet \geq 0 \\ 0 & \bullet < 0 \end{cases}$$

In these equations, Λ represents the nonlinearity introduced by the check valves. Typically, to account for both laminar and turbulent flow regimes, the flow coef-

ficients vary as a function of the Reynolds number. Since the relationship expressed in Eq. 1 is based on a turbulent flow regime, K_v must depend on the square root of ΔP for laminar flow regimes. Hence, the approach used herein is to have a lookup table that computes the flow coefficients based on the pressure differential across the orifice.

The variable flow models are accounted for in Eq. 11 and Eq. 12, where the former corresponds to the pilot flow and the latter corresponds to the main flow. The variable σ represents the flow mode (*i.e.* forward or reverse).

$$Q_{PC} = K_{VPC}(y_p - y_c) \operatorname{sgn}(P_p - P_c) \sqrt{|P_p - P_c|} \quad (11)$$

$$Q_{AB} = K_{VAB}(y_{mp}, \sigma) \operatorname{sgn}(P_A - P_B) \sqrt{|P_A - P_B|} \quad (12)$$

The flow coefficients $K_{VPC}(\cdot)$ and $K_{VAB}(\cdot)$ are difficult to estimate analytically (Johnston et al., 1991). This is particularly true in this case because of the singular geometry of the head of the main poppet and the flow path around the pilot stage. In this paper, the K_{VAB} coefficient is obtained experimentally and the K_{VPC} coefficient is obtained from Computational Fluid Dynamics analyses (CFD).

The dynamics of the pressure chambers are modeled by the following equations in which an effective bulk modulus β_c is accounted for as suggested by (Watton, 1989). Notice that temperature effects are neglected.

$$\dot{P}_p = \frac{\beta_c}{V_p} (Q_{AP} + Q_{BP} - Q_{PC} - Q_{PH} - \dot{V}_p)$$

$$\dot{P}_c = \frac{\beta_c}{V_c} (Q_{PC} - Q_{CA} - Q_{CB} - \dot{V}_c) \quad (13)$$

$$\dot{P}_h = \frac{\beta_c}{V_h} (Q_{PH} - \dot{V}_h)$$

The corresponding volumes of each chamber are given in Eq. 14 and their rates of change with respect to time can be easily obtained by differentiation. In these equations, $V_i(0)$ denotes the corresponding initial volume.

$$V_p = V_p(0) + (A_{p\text{low}} + A_o)y_p - A_{c\text{up}}y_c - A_{m\text{pup}}y_{mp}$$

$$V_h = V_h(0) - A_{p\text{up}}y_p \quad (14)$$

$$V_c = V_c(0) - A_{m\text{plow}}y_{mp} + (A_{c\text{low}} + \alpha A_o)y_c$$

In this equation, α is a parameter to designate the contact state between the piston and the pilot pin.

$$\alpha = \begin{cases} 0 & (y_p - y_c) \geq 0 \\ 1 & (y_p - y_c) < 0 \end{cases} \quad (15)$$

The output flow of the EHPV is given by the addition of the main flow and the active pilot flow (active in the sense of flow direction) as specified in

$$Q_{\text{out}} = \begin{cases} Q_{CB} + Q_{AB} - Q_{BP} & \text{forward flow} \\ -Q_{CA} + Q_{AB} + Q_{AP} & \text{reverse flow} \end{cases} \quad (16)$$

Finally, the output of the valve is expressed as the valve's flow conductance coefficient K_v ,

$$K_v = \frac{|Q_{out}|}{\sqrt{|P_A - P_B|}} = \frac{|Q_{out}|}{\sqrt{|\Delta P|}} \quad (17)$$

4 Experimental Technique

Some of the parameters needed for the model of the valve can be easily measured with standard laboratory equipment, or can be requested from the manufacturer. These include geometrical parameters, masses, and spring preloads. Others such as the solenoid force, the stiffness of springs, flow coefficients, flow forces, and friction require some effort and are presented next.

The solenoid force is found by measuring the force needed to maintain the armature-pilot at different positions while fixing the current. The data are presented in Fig. 4.

The stiffness values of the springs can be computed from the force vs. displacement characteristics shown in Fig. 5. Notice that the tubular spring possesses a large stiffness. In addition, it is important to mention that the modulating spring is always operated in the linear region because of its preload. This fact also applies to the bias spring. Typically, the stiffness of the bias spring, k_b , is around 4000 N/m.

The flow coefficient of the main poppet K_{vAB} is presented in Fig. 6 as a function of the main poppet displacement y_{mp} for forward flow. This parameter is estimated by locking the main poppet at different positions and recording the flow through the valve and the pressure difference across the same⁴. To simplify the model, it is assumed that the pressure atop the pilot P_h is always the same as that of the control pressure chamber P_p . Thus, K_{vPH} is assumed to be sufficiently large. The flow conductance values for the other internal orifices are also given in Fig. 6. The data shown in these figures were obtained from extrapolation of measured steady state data.

Flow forces are difficult to estimate analytically for this valve. Literature shows that although theoretical predictions of flow forces and flow coefficients for simple geometries agree qualitatively well with experimental results, poor quantitative agreement has been reported (Johnston et al., 1991). The estimated static flow forces affecting the main poppet and pilot pin are displayed in Fig. 7. For the main poppet, the flow forces, obtained experimentally, are shown as function of displacement at several pressure differentials. The flow forces affecting the pilot are also shown in this figure. These were obtained via CFD analyses, a method previously used in (Yang, 2004). In these plots, positive values denote closing forces acting on the corresponding elements. Note that the flow forces for the compensating piston are ignored.

Friction forces for the poppet and the armature-pilot

body are obtained by measuring the force needed to cause an initial displacement. For these mechanical elements, this type of Coulomb friction results from the contact between the seals and the walls of the valve. Moreover, these friction forces are affected by the pressure difference across the seal. The data presented in Table 1 applies to the main poppet element. Note that in this table $\lambda = |P_A - P_p|$. It is assumed that the friction in the pilot stage is negligible.

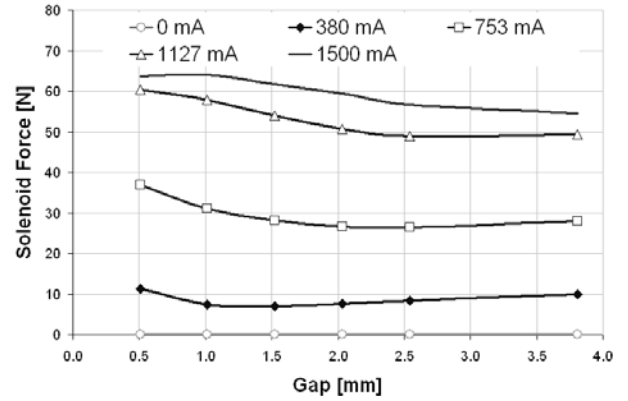


Fig. 4: Magnetic force of the solenoid of the EHPV

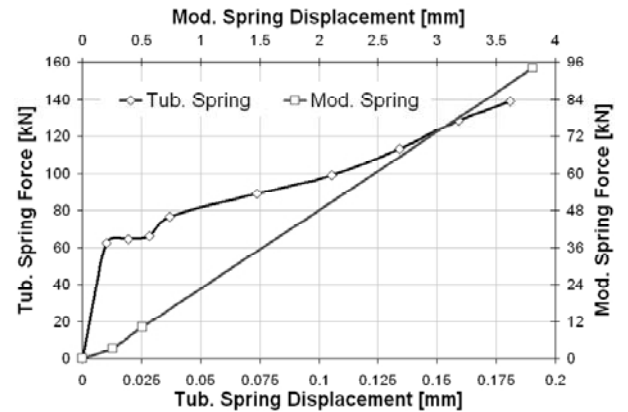


Fig. 5: Modulating spring and tubular spring force vs. displacement characteristics

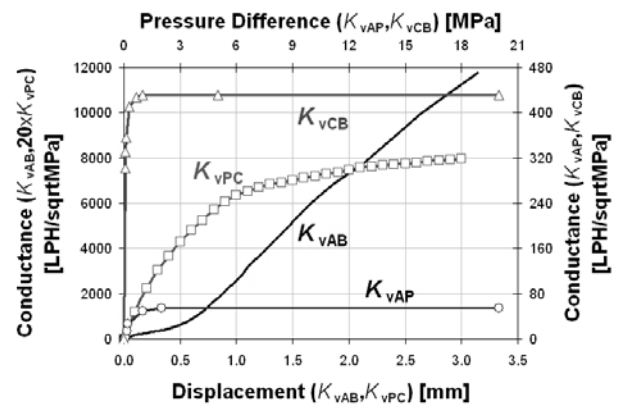


Fig. 6: Characteristics of internal flow conductance factors

⁴ The trends seen in the data for the K_{vAB} coefficient are due to the particular geometry of the poppet element in this valve.

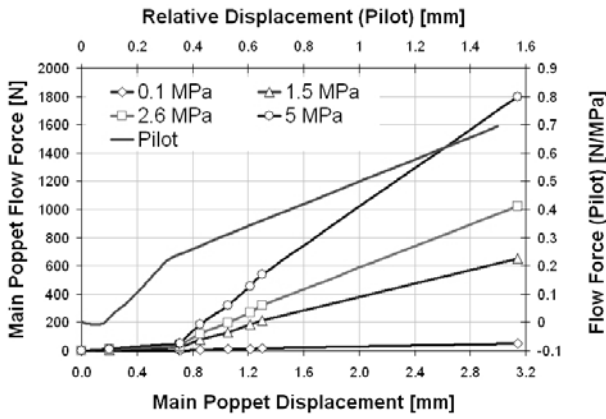


Fig. 7: Main poppet and pilot pin flow forces

Table 1: Seal friction as a function of pressure difference

λ (MPa)	Friction Force (N)
0	10.76
0.7	12.66
2.5	20.33
5.0	28.34
10.0	32.45
15.0	39.23
22.5	45.91
30.5	55.91

The position of the main poppet and the pilot were not available during the transient response of the valve. This complicates the estimation of the damping coefficients. However, from knowing K_{vAP} , P_A and P_p , then the pilot flow Q_{AP} can be established from Eq. 10. Furthermore, P_c can also be computed using this equation if K_{vCB} and P_B are known. With this information, one can compute the main flow Q_{AB} from knowledge of the output flow Q_{out} . Consequently, y_{mp} can be estimated numerically using Eq. 12 if K_{vAB} is known. In the event $y_c = y_{mp}$, then y_p can also be computed from Eq. 11 with knowledge of K_{vPC} . This procedure was utilized to obtain estimated responses for the position of the main poppet and the pilot pin. The damping coefficients were then determined by minimizing the error between the estimated responses and the predicted ones. These values are given in Table 2.

It is worth mentioning that all of the experimental data provided previously are used in the model via look-up tables.

Table 2: Values for the different viscous friction coefficients

Var.	Description	Value	Units
b_b	Bias spring visc. damping coeff.	1.20	Ns/m
b_p	Mod. spring visc. damping coeff.	1004	Ns/m
b_{mp}	Main poppet visc. damping coeff.	502	Ns/m

5 Nonlinear Model Validation

Several step responses were used to obtain a time domain validation of the nonlinear model discussed above. Step voltages were sent to an operational amplifier which converted the signals from 940 mA to 1250 mA. The current out of the amplifier was sent to the solenoid of the EHPV at the same time that it was recorded for analysis. Data from the inlet, pilot, and outlet pressures of the EHPV were also recorded along with fluid flow measurements. A custom made orifice-type flowmeter was employed for this purpose. This meter was calibrated with steady state flow data from a turbine-type flowmeter taking into account temperature and pressure difference data. The noise content of the data was smoothed offline using a mean filter. The results are plotted in Fig. 8 for the forward flow direction.

In Fig. 8, a comparison is shown between the recorded and the modeled response of the flow conductance parameter. The mean value of the prediction error was computed as $-2.20 \text{ LPH/MPa}^{1/2}$ with a standard deviation of $75.3 \text{ LPH/MPa}^{1/2}$. In addition, the comparison between the recorded and the modeled responses of the relevant pressures is shown in this figure as well. Note that a value of $6.89 \times 10^2 \text{ MPa}$ was used for the effective bulk modulus β_c .

It is important to mention that when running the model in SIMULINK, a considerable amount of computation time was experienced. This is due to the stiff nature of the differential equations describing the behavior of the EHPV.

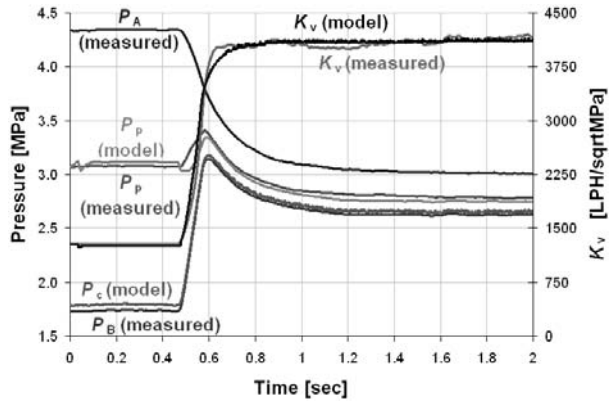


Fig. 8: Actual and modeled step response of the EHPV

6 Proposed Reduced Order Model

Although the nonlinear model is computationally expensive, it can be used to gain insight about performance improvements, which will be explored in a future paper. Nonetheless, from observations on the collected experimental data, a simplified model can be used to predict the opening response of the EHPV. This simplified model can then facilitate the development of control algorithms for this valve. This simplified model is constructed as a Hammerstein model. In other words, this simplified model uses a linear time invariant sec-

ond order parametric model with a static nonlinear input gain Γ . Moreover, the input to the model is the current sent to the solenoid i_{sol} , and the output of the model is the valve's flow conductance parameter K_v . This is shown in Eq. 18.

$$\ddot{K}_v + 2\zeta\omega_n\dot{K}_v + \omega_n^2 K_v = \omega_n^2 \Gamma(i_{sol}, \Delta P, \sigma) \quad (18)$$

In this model, the variable ΔP represents the pressure drop across the valve and the variable σ represents the flow mode (*i.e.* forward or reverse). The nonlinear input gain Γ is realized from steady state flow conductance data. For example, typical steady state flow conductance characteristics for the reverse flow mode are given in Fig. 9. This plot shows the flow conductance as function of pressure drop at different input currents⁵. Notice that the sensitivity of dynamic parameters to pressure difference across the valve is ignored in this model.

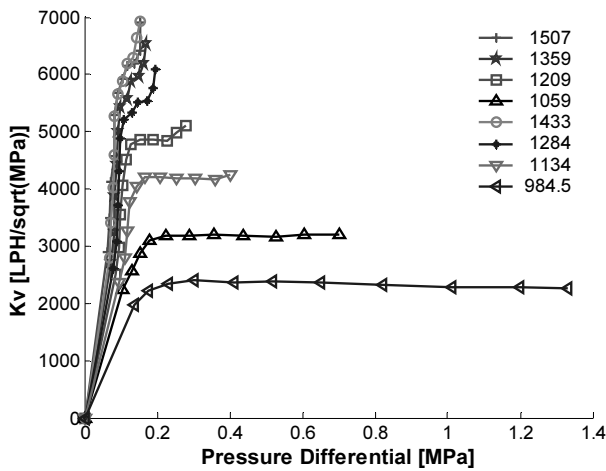


Fig. 9: Steady state reverse flow conductance as a function of pressure drop at different solenoid currents

Experimental data were collected to estimate the dynamic part of the model. The damping ratio ζ and the natural frequency ω_n were estimated by minimizing the error between the collected data and the corresponding prediction of the model. The estimated coefficients are given in Table 3 and are valid in the range 0.6 to 6.5 MPa.

Table 3: Dynamic parameters for the simplified EHPV model

Var.	Description	Value	Units
ζ	Damping ratio	1.25	-
ω_n	Natural frequency	72.1	rad/s

It can be noticed in Fig. 9 that for pressure differentials greater than 0.4 MPa, the flow conductance parameter is merely a function of the input current. If a minimum pressure difference (higher than this value) is always maintained across the valve, then one can take advantage of the independence of K_v from ΔP . If this is the case, the model can be further simplified as

$$\ddot{K}_v + 2\zeta\omega_n\dot{K}_v + \omega_n^2 K_v = \omega_n^2 \tilde{\Gamma}(i_{sol}, \sigma) \quad (19)$$

where $\tilde{\Gamma}$ is computed from the data given in Table 4.

The comparison of the experimental data and the prediction from the simplified models are given in Fig. 10. The response of the EHPV under reverse flow mode uses Eq. 18 while that under forward flow mode uses Eq. 19. The initial nominal pressure difference for the forward flow data is 2.5 MPa. The final nominal pressure is 1.5 MPa for 994 mA and 1.1 MPa for 1092 mA. The initial nominal pressure difference for the reverse flow data is 1.8 MPa. The final nominal pressure is 0.4 MPa for 1147 mA and 0.2 MPa for 1503 mA. The experimental data is filtered offline with a mean filter for presentation purposes. Note that the data appears noisier for high values of input current. This is a consequence of the proximity of the pressure differential values to the resolution of the pressure sensors (0.05 MPa).

Table 4: Simplified steady state gain for the EHPV

Forward Flow ($\sigma = 1$)		Reverse Flow ($\sigma = -1$)	
i_{sol} (mA)	$\tilde{\Gamma}$ (LPH/sqrtMPa)	i_{sol} (mA)	$\tilde{\Gamma}$ (LPH/sqrtMPa)
0	0	0	0
500	10	575	176
583	16	568	151
660	310	626	255
750	330	850	1051
830	500	900	1500
916	1000	984	2265
1000	1833	1058	3205
1100	3070	1133	4244
1250	5100	1207	5099
1318	6080	1282	5980
1398	7006	1357	6602
1483	8002	1431	7120
1500	8216	1500	7731

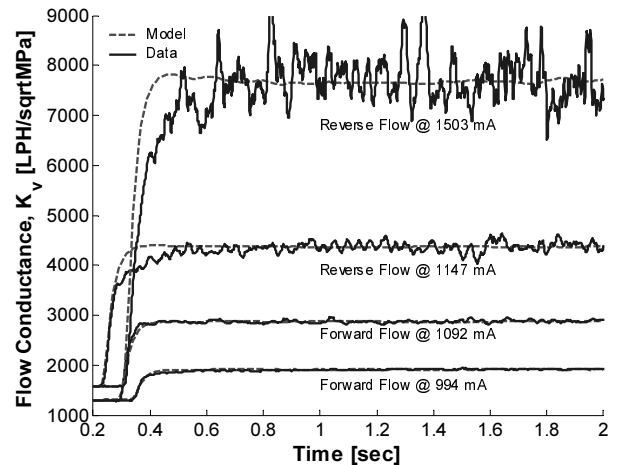


Fig. 10: EHPV actual and modeled step responses for the forward flow conductance

⁵ The data were collected at a nominal temperature of 42°C. Temperature effects are neglected herein.

7 Conclusions

A nonlinear mathematical model has been presented for the EHPV. The model is based on the interactions among the valve's internal systems: mechanical, electromagnetic, and hydraulic. The complexity of the model resides on the mechanical constraints, flow force characteristics, nonlinear flow models, bidirectionality, and electromagnetic nonlinearities. It is important to remark that the resulting model is computationally expensive. However, it can be used in the future to gain further insight about the valve's stability and performance improvements or limitations. From observations on the collected experimental data, a simplified model was proposed. This model is composed by a linear second order system with a static input nonlinearity. This nonlinearity is realized with steady state flow conductance data. When the pressure difference across the EHPV is sufficiently high and does not change considerably, this input nonlinearity can be simplified. The resulting separation of nonlinear effects and linear dynamics could be used in the design of a control scheme for the valve based on inverse linearisation. This will be explored in a future paper. The effectiveness of the models was successfully evaluated through experimental validation. Note that throughout this paper, temperature effects on the flow conductance of the valve are neglected. This is applicable provided that extreme changes in oil temperature are not considered.

Acknowledgments

The authors gratefully acknowledge the support provided to this project by HUSCO International and the Fluid Power Motion Control Center. This project was concluded while the first author was a Ph.D. candidate in the School of Mechanical Engineering at Georgia Tech.

Nomenclature

A_A	Effective area port A	[mm ²]
A_B	Effective area port B	[mm ²]
b_b	Bias spring viscous friction coef.	[Ns/m]
b_c	Tubular spring viscous friction coef.	[Ns/m]
b_{mp}	Main poppet viscous friction coef.	[Ns/m]
b_p	Modulating spring viscous friction coef.	[Ns/m]
F_{sol}	Solenoid force	[N]
i_{sol}	Solenoid current	[mA]
k_b	Bias spring stiffness	[N/m]
k_c	Tubular spring stiffness	[N/m]
k_p	Modulating spring stiffness	[N/m]
P_A	Pressure port A	[MPa]
P_B	Pressure port B	[MPa]
P_c	Pressure in compensation chamber	[MPa]
P_h	Pressure in pilot head chamber	[MPa]
P_p	Pressure in control pressure chamber	[MPa]
Q	Hydraulic oil flow	[LPH]
V_c	Oil volume in compensation chamber	[L]

V_h	Oil volume in pilot head chamber	[L]
V_p	Oil volume in control pressure chamber	[L]
y_c	Compensating piston position	[m]
y_{mp}	Main poppet position	[m]
y_p	Pilot-Armature position	[m]
β_e	Effective bulk modulus	[MPa]
ω_n	Natural frequency	[rad/s]
ζ	Damping ratio	

References

- Du, H.** 2002. An E/H control design for poppet valves in hydraulic systems. *ASME The Fluid Power and Systems Technology Division*, Vol. 9, pp. 141-148.
- Fales, R.** 2006. Stability and performance analysis of a metering poppet valve. *International Journal of Fluid Power*, Vol. 7, pp. 11-17.
- Hayashi, S.** 1995. Instability of poppet valve circuit. *JSME International Journal, Series C (Dynamics, Control, Robotics, Design and Manufacturing)*, Vol. 38, pp. 357-66.
- Johnston, D. N., Edge, K. A. and Vaughan, N. D.** 1991. Experimental investigation of flow and force characteristics of hydraulic poppet and disc valves. *Proceedings of the Institution of Mechanical Engineers, Part A: Power and Process Engineering*, Vol. 205, pp. 161-171.
- Kajima, T. and Kawamura, Y.** 1995. Development of a high-speed solenoid valve: investigation of solenoids. *IEEE Transactions on Industrial Electronics*, Vol. 42, pp. 1-8.
- Kitagawa, A., Sanada, K. and Pingdong, W.** 1998. A study on proportional control of flow rate by a PWM-controlled logic valve. *Transactions of the Japan Hydraulics and Pneumatics Society*, Vol. 29, pp. 53-57.
- Liu, S., Krutz, G. and Yao, B.** 2002. Easy5 model of two position solenoid operated cartridge valve. *ASME The Fluid Power and Systems Technology Division*, Vol. 9, pp. 63-67.
- Opdenbosch, P., Sadegh, N. and Book, W. J.** 2004. Modeling and control of an electro-hydraulic poppet valve. *ASME The Fluid Power and Systems Technology Division*, Vol. 11, pp. 103-110.
- Roberts, B. J.** 1988. Poppet Valves for Directional control. *Machine Design*, Vol. 60, pp. 119-22.
- Shin, Y. C.** 1991. Static and Dynamic Characteristics of a Two-Stage Pilot Relief Valve. *Transactions of the ASME. Journal of Dynamic Systems, Measurement and Control*, Vol. 113, pp. 260-268.
- Tabor, K. A.** 2004. Velocity Based Method of Controlling an Electrohydraulic Proportional Control Valve. *U.S. Patent No. 6,775,974*.
- Vaughan, N. D. and Gamble, J. B.** 1996. The modeling and simulation of a proportional solenoid valve.

Transactions of the ASME. Journal of Dynamic Systems, Measurement and Control, Vol. 118, pp. 120-5.

Vaughan, N. D., Johnston, D. N. and Edge, K. A. 1992. Numerical simulation of fluid flow in poppet valves. *Proceedings of the Institution of Mechanical Engineers, Part C: Mechanical Engineering Science*, Vol. 206, pp. 119-127.

Watton, J. 1989. *Fluid power systems: modeling, simulation, analog and microcomputer control*, New York, Prentice Hall.

Yang, R. 2004. Predicting hydraulic valve flow forces using CFD. *ASME The Fluid Power and Systems Technology Division*, Vol. 11, pp. 55-61.

Yang, X., Pfaff, J. L. and Paik, M. J. 2004. Pilot Operated Control Valve having a Poppet with Integral Pressure Compensating Mechanism. *U.S. Patent No. 6,745,992*.

Yang, X., Stephenson, D. B. and Paik, M. J. 2001. Bidirectional Pilot Operated Control Valve. *U.S. Patent No. 6,328,275*.

Zhang, R., Alleyne, A. G. and Prasetyawan, E. A. 2002. Performance limitations of a class of two-stage electro-hydraulic flow valves. *International Journal of Fluid Power*, Vol. 3, pp. 47-53.



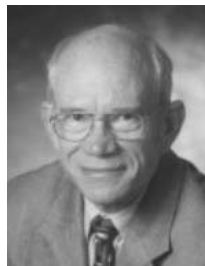
Patrick Opdenbosch, Ph.D.

Dr. Opdenbosch received the Bachelor of Science in Mechanical Engineering from the Georgia Institute of Technology in 2002. He also received the M.S. and Ph.D. degrees in 2005 and 2007 respectively from the same university. Currently, he is a controls engineer at Caterpillar Inc. His research interests include intelligent control applied to fluid power, fault diagnostics, robotics, mechatronics, and machine vision.



Nader Sadegh, Ph.D.

Professor Sadegh received the Bachelor of Science in Mechanical Engineering from the University of California, Santa Barbara in 1982. He received the M.S. and Ph.D. degrees in 1984 and 1987 respectively from the University of California, Berkeley. He is currently an Associate Professor at the Georgia Institute of Technology. His research interests include nonlinear identification and control, neural networks, robotics, and adaptive control.



Wayne Book, Ph.D.

Professor Book received the Bachelor of Science in Mechanical Engineering from the University of Texas, Austin in 1969. He received the M.S. and Ph.D. degrees in 1971 and 1974 respectively from the Massachusetts Institute of Technology. He is currently the HUSCO/Ramirez Chair in Fluid Power at Georgia Tech. His research interests include the design, dynamics, and control of light weight motion systems, robotics, fluid power, and haptics. He is a fellow of the ASME, SME, and IEEE, and received the Georgia Tech's award for Outstanding Faculty Leadership for development of graduate research assistants in 1987, and an ASME dedicated Service award in 2003 and the ASME DSCD Leadership award in 2004.



Todd Murray

Mr. Murray received the Bachelor of Science in Mechanical Engineering from the University of Wisconsin at Milwaukee in 2003. He has been employed at HUSCO International since, and worked as a Controls and Simulation Engineer, specializing in EHPV modeling, from 2004 to 2007. His professional interests also include on-highway suspension systems, and he is currently developing adaptive damping automotive suspension hardware.



Roger Yang, Ph.D.

Dr. Yang received the Bachelor of Science in Mechanical Engineering from Shanghai University of Technology, China in 1982. He received the Ph.D. degree of Mechanics in 1991 from University of Minnesota, Minneapolis. He is currently a Senior Staff Engineer at HUSCO International, Inc. His research interests include R&D in hydraulic valve systems and advanced computer simulations in mobile hydraulics.